International Biodeterioration & Biodegradation 97 (2015) 115–123

Contents lists available at ScienceDirect

International Biodeterioration & Biodegradation

journal homepage: www.elsevier.com/locate/ibiod

A coupled photocatalytic-biological process for phenol degradation in the *Phanerochaete chrysosporium*-oxalate-Fe_3O_4 system

Dan-Lian Huang [a, b, *], Cong Wang [a, b], Piao Xu [a, b], Guang-Ming Zeng [a, b, *], Bing-An Lu [c], Ning-Jie Li [a, b], Chao Huang [a, b], Cui Lai [a, b], Mei-Hua Zhao [a, b], Juan-Juan Xu [a, b], Xiang-Ying Luo [a, b]

[a] College of Environmental Science and Engineering, Hunan University, Changsha 410082, PR China
[b] Key Laboratory of Environmental Biology and Pollution Control (Hunan University), Ministry of Education, Changsha 410082, PR China
[c] Key Laboratory for Micro-Nano Optoelectronic Devices (Hunan University), Ministry of Education, Changsha 410082, PR China

ARTICLE INFO

Article history:
Received 8 June 2014
Received in revised form
8 October 2014
Accepted 3 November 2014
Available online

Keywords:
Degradation
Enzymes
Fe_3O_4 nanoparticles
Filamentous fungi
Oxalate
Phenol

ABSTRACT

A novel composite system, containing Fe_3O_4 nanoparticles and *Phanerochaete chrysosporium* together with its secretion oxalate, was developed for phenol degradation. Fe_3O_4 played an important role in the composite system as they could efficiently enhance phenol degradation when coexisted with oxalate under light. The maximal phenol degradation efficiency (93.41%) under solar light was detected at 0.5 g L^{-1} Fe_3O_4, while it reached a peak (40.36%) at 0.7 g L^{-1} Fe_3O_4 under dark. Additionally, oxalate was found to be strongly dependent on Fe_3O_4 nanoparticles concentration, ranging from 26.27 to 32.78 mM. And adequate oxalate could enhance phenol degradation due to the participation of oxalate in the photocatalytic process. Furthermore, phenol degradation efficiency increased with the increase of phenol concentration. Besides, the contribution of manganese peroxidase (MnP) to phenol degradation was greater than that of lignin peroxidase (LiP). Cluster analysis indicated that MnP and oxalate could be the main factors that influenced phenol degradation. Importantly, both the biodegradation and photocatalysis played part in the degradation process. These findings proposed a new method of treatment of phenol wastewater and could provide useful references for more efficient treatment of phenol wastewater.

Introduction

Phenolic compound, is one of the 129 kinds of precedence-controlled pollutants set by Environmental Protection Agency (EPA). Phenol is usually referred as model compound in wastewater research because it is the primary water contaminants in the environment (Shaari et al., 2012). Phenol is toxic either by ingestion or by contact or inhalation even at low concentrations. Acute exposure to phenol causes central nervous system disorders, which leads to collapse and coma (Nair et al., 2008). And it is often contained in wastewater from oil refineries, coal gasification plants and phenol resin industry and is most frequently found in polluted rivers and industrial effluents (Martínková et al., 2009). Besides, discharging of wastewater containing phenol into receiving bodies of water endangers aquatic life, even at relatively low phenol concentrations (Kibret et al., 2000; Chung et al., 2003). Therefore, the removal of phenol from industrial wastewater is of great practical significance for the environmental protection.

In recent years, due to the advantage of high surface area to volume ratios and unique superparamagnetism, the synthesis and utilization of iron oxide nanoparticles (Fe_3O_4 NPs) with novel properties and functions have been widely investigated (McHenry and Laughlin, 2000; Afkhami et al., 2010; Pan et al., 2010). In particular, it is noticeable that iron oxide nanoparticles have also shown considerable potential as photocatalysts to break down or to convert pollutants into a less toxic form even under visible light (Leland and Bard, 1987; Xu et al., 2012a). Furthermore, iron oxide coexists with oxalate can set up a photo-Fenton-like system via the formation of attractive hydroxyl radicals (•OH) without external H_2O_2 compared with traditional Fenton system (Siffert and

* Corresponding authors. College of Environmental Science and Engineering, Hunan University, Changsha 410082, PR China. Tel.: +86 731 88822754; fax: +86 731 88823701.
E-mail addresses: huangdanlian@hnu.edu.cn (D.-L. Huang), zgming@hnu.edu.cn (G.-M. Zeng).

http://dx.doi.org/10.1016/j.ibiod.2014.11.001
0964-8305/

Sulzberger, 1991; Faust and Zepp, 1993; Lei et al., 2006). Iron oxides are mainly acted as a photocatalyst, while oxalate can be excited to generate electron–hole pairs (Leland and Bard, 1987; Siffert and Sulzberger, 1991). Photo-Fenton-like system with the existence of iron oxides and oxalate can provide a promising and effective method for photocatalysis of organic pollutants, possessing tremendous application potential in wastewater treatment. It is important that iron oxide can be used as immobilization carrier to remove pollutants. Xu et al. (Xu et al., 2012b, 2013) used iron oxide magnetic nanoparticles and Ca-alginate immobilized white rot fungus to remove Pb(II) ions and achieved high adsorption efficiencies, which also showed that iron oxide possessed low toxicity and favorable biocompatibility and could be applied in wastewater treatment when combined with white rot fungus.

Numerous studies about the degradation of pollutants by white rot fungus have been conducted in recent years. *Phanerochaete chrysosporium* (*Pc*), one of the white rot fungus, can secrete a group of hemoperoxidases in response to nutrients limitation during their secondary metabolism, namely lignin peroxidase (LiP) and manganese peroxidase (MnP) (Huang et al., 2006, 2008, 2010a, 2010b; Zhao et al., 2012; Lai et al., 2013). These enzymes can catalyze the degradation of a wide variety of organic pollutants (Bumpus et al., 1985; Barr and Aust, 1994). Besides, it has been reported that *Pc* can secrete oxalate during its growth in both liquid and solid culture medium (Dutton et al., 1993; Galkin et al., 1998; Mäkelä et al., 2002). In previous studies, most attention has been paid to the treatment of wastewater by fungi or photo-Fenton-like system. However, to our best knowledge, no details on the degradation of phenol wastewater in the system consisting of Fe_3O_4 NPs and fungi together with its secretion oxalate have been reported so far. This study will help us to understand the phenol degradation in the composite system contained Fe_3O_4 NPs and *Pc* together with its secretion oxalate, which would provide useful information for the effective treatment of phenol wastewater.

The primary aim of this study was to investigate the phenol wastewater degradation under the action of Fe_3O_4 NPs and white rot fungus along with its secretion oxalate. Also, the different quantity of Fe_3O_4 NPs and initial phenol concentrations, oxalate production were discussed. Besides, two main ligninolytic enzymes, LiP and MnP, secreted by *Pc* (BKMF-1767) were determined to follow their connection with the degradation of phenol.

Material and methods

Strains

A white rot fungus, *Pc* strain (BKMF-1767), purchased from the China Center for Type Culture Collection (CCTCC), was used in this study. It was maintained at low temperature 4 °C on potato dextrose agar (PDA) slants and then transferred to PDA plates at 30 °C for 7 days. Inocula consisted of spore suspension which was prepared by scraping the spores on the agar surface and then diluting them in sterile distilled water. Spore concentration was measured and adjusted to 5.33×10^5 CFU mL^{-1}. To obtain the inoculum, we used the medium as previously described by Kirk et al. (Kirk et al., 1978).

Synthesis of Fe_3O_4 nanoparticles

9.7936 g of $FeCl_3 \cdot 6H_2O$, 5.5980 g of $FeSO_4 \cdot 7H_2O$ and 1.6775 mL of HCl (12 M) were dissolved in 50 mL of ultrapure water (degassed with nitrogen gas before use). Then, the solution was added dropwise into 300 mL of 1.5 M NaOH solution under vigorous stirring using nonmagnetic stirrer at 70 °C. The obtained Fe_3O_4 NPs were separated from the reaction medium by magnetic field, and washed four times with 200 mL ultrapure water, then resuspended in 150 mL ultrapure water.

Degradation procedure under light and dark condition

The degradation of phenol in the composite system, which contained Fe_3O_4 NPs and white rot fungus (*Pc*) together with its secretion oxalate, was investigated in conical flask tests under solar light (YZ08-T5 three-band fluorescent lamp, the light intensity was about 200 lux) and dark condition. For comparison, samples without Fe_3O_4 NPs suspension, only Fe_3O_4 NPs suspension, Fe_3O_4 NPs-oxalate system were experimented as the same. 2.0 mL spore suspension was added to Kirk liquid culture medium (sterilized under 115 °C for 30 min before use) with a given Fe_3O_4 NPs levels of 0.1, 0.3, 0.5, 0.7, 1.0 and 1.5 g L^{-1}, and then cultured under 30 °C and 150 rpm for 3 d at both light and dark conditions. Then, a certain amount of sterilized phenol solution was added to the suspension system (the initial concentrations of phenol were 60 mg L^{-1}), and cultured for another 3 d. At given time intervals (24 h), the analytical samples were taken from the suspension system and immediately centrifuged at 9, 000 rpm for 10 min, then filtered through 0.45 μm membrane filter. The substrate filtrate was stored for analysis.

In order to investigate the effect of initial concentration of phenol on the degradation ability, various concentrations of phenol were conducted. All of the Fe_3O_4 NPs levels were 0.5 g L^{-1}, and initial phenol concentrations were 0, 20, 40, 60, 80, 100 and 120 mg L^{-1}, respectively. All experiments were performed in three replicates.

Characterization

In order to study the shape and size distribution of Fe_3O_4 NPs after synthesis, Fe_3O_4 NPs were visualized by electron microscopy. Zeta potentiometer (Mastersizer 2000) was used to measure the size of nanoparticles. The Fe_3O_4 nanoparticles suspension was centrifuged at 20 °C, 4000 rpm for 5 min. After that, the Fe_3O_4 NPs were freeze dried for 12 h. The particle size and morphology of the synthesized NPs were determined by a scanning electron microscope (SEM) model (Hitachi S4800).

Analysis of biomass

At given time intervals (24 h), the *Pc* hyphae pellet was took out from the medium and washed several times with ultrapure water, then the weight was measured after heated at 60 °C for 48 h.

Enzyme activities assays

The extracellular non-specific and non-stereoselective ligninolytic system of *Pc* is composed of LiP and MnP, which function together with H_2O_2 producing oxidases and secondary metabolites (Singh and Pakshirajan, 2010).

Two main ligninolytic peroxidases, LiP and MnP, were measured with a Shimadzu 2550 UV–visible spectrophotometer in this study. LiP activity was measured by a modified method as described by Tien and Kirk (Tien, 1988), with one unit (U) representing 1 μmol of veratryl alcohol oxidized to veratraldehyde per minute at pH 3.0 and 25 °C. Each reaction mixture (total volume 3 mL) contained 1.5 mL of 100 mM sodium tartrate (pH 3.0), 1 mL of 10 mM veratryl alcohol, 0.4 mL of enzyme extract, and the reaction was started with the addition of 0.1 mL H_2O_2 (10 mM). The formation of veratraldehyde was monitored at 310 nm ($\varepsilon_{310} = 9300$ mol^{-1} cm^{-1}).

MnP activity was determined according to the method described by Wariishi et al. (Wariishi et al., 1992), which was based

on the oxidation of Mn^{2+} to Mn^{3+}. Each 3-mL reaction mixture contained 2.4 mL of 50 mM sodium succinate (pH 4.5), 0.1 mL of 15 mM $MnSO_4$, 0.4 mL of crude enzyme solution, and the reaction was started with the addition of 0.1 mL H_2O_2 (10 mM) and initiated at 37 °C. The rate of Mn^{3+}-succinate complex formation was monitored by measuring the increase in absorbance at 240 nm ($\varepsilon_{240} = 8100\ mol^{-1}\ cm^{-1}$).

Oxalate production analysis

Oxalate in the substrate filtrate was analyzed by high performance liquid chromatography (HPLC) using an Agilent 1100 apparatus equipped with UV–vis variable wavelength detector (VWD). Phosphoric acid (0.15% v/v) was used as the solvent at a flow rate of 0.5 mL min^{-1}, and detection wavelength was 210 nm. The column was maintained at 30 °C.

Phenol analytical methods

Phenol concentration in the culture was determined by a colorimetric method based on rapid condensation with 4-aminoantipyrene (4-AAP), followed by oxidation with potassium ferricyanide under alkaline conditions to give a redcolored product. To measure phenol concentration, a Shimadzu 2550 UV–visible spectrophotometer was used to determine the absorbance at a wavelength of 510 nm. Prior to the measurement, a calibration curve was obtained using standard phenol solution (from 0 to 7 mg L^{-1}) and a good linear relationship was shown between absorbance and phenol concentration.

Analysis of hydroxyl radicals

The improved thiobarbituric acid (TBA) method was used to assay •OH (Halliwell et al., 1985). TBA-reactive substances (TBARS) were determined as follows. 0.0022 g 2-deoxy-D-ribose was added into 4 mL filtrate and incubated at 37 °C for 1 h, then TBA (Sigma, 0.25%) and trichloroacetic acid (0.7%) were added, and the mixture was heated at 100 °C for 15 min. The absorbance at 532 nm was measured. The control was the same reaction mixture with no sample leach liquor added. The reductive activity of •OH was indicated by the decrease of absorbance at 532 nm compared to that of the control.

Statistical analysis

The results to be presented were the mean values of three replicates. Standard deviation and error bars were indicated wherever necessary. Statistical analyses were performed to obtain more comprehensive and useful information, using the software package SPSS 19.0 for Windows (SPSS, Germany). Cluster analysis was conducted to classify four indexes (degradation efficiency, oxalate concentration, LiP activity and MnP activity) at different phenol concentrations based on the calculation of similarity measures between the values of different indexes in one group and those in another group. Between-groups linkage was used as cluster method.

Results and discussion

Characterization of Fe_3O_4 NPs

In order to get more direct information about morphology of prepared Fe_3O_4 NPs, SEM was employed to observe the morphologies at the nanometer level of Fe_3O_4 NPs (Fig. 1a and b) and zeta potentiometer was used to measure the size of nanoparticles

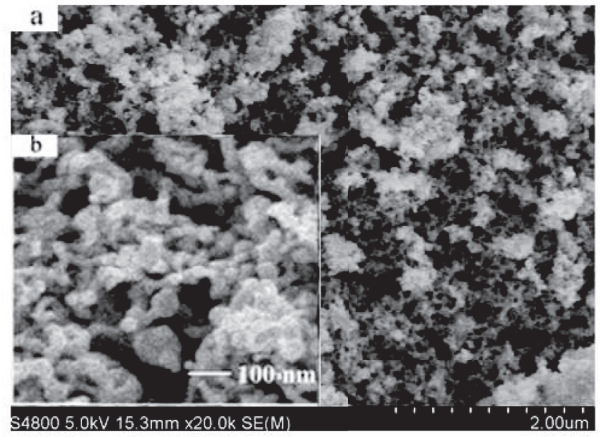

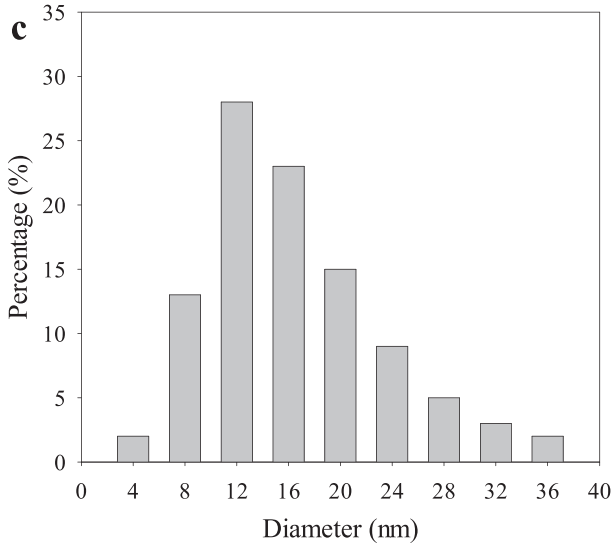

Fig. 1. SEM images of the morphologies of Fe_3O_4 NPs (a and b) and size distribution of Fe_3O_4 NPs (c).

(Fig. 1c). As seen in Fig. 1a and b, the micrograph revealed that NPs were in infinitesimal size and displayed a little agglomerate. Besides, the NPs were spherical in shape and formed small clusters mainly due to magnetic nature of the Fe_3O_4 NPs. The surface of the spheres exhibited morphologically rough and irregular and composed of many small nanoparticles. The average sizes of Fe_3O_4 particles were in the range of 8–20 nm.

Biomass

The biomass in the treatments with different materials (*Pc*; *Pc* and 60 mg L^{-1} phenol; *Pc* and 0.5 g L^{-1} Fe_3O_4; *Pc*, 0.5 g L^{-1} Fe_3O_4 and 60 mg L^{-1} phenol; *Pc*, 0.5 g L^{-1} Fe_3O_4 and 120 mg L^{-1} phenol) varied during degradation process (Fig. 2). The results displayed that the biomass increased with the increase of time, and the biomass concentrations in the treatments contained *Pc* and Fe_3O_4 NPs were higher than the treatments only contained *Pc* when phenol was not added in (day 0 of Fig. 2), which was ascribed to the fact that Fe_3O_4 NPs covered on the surface of *Pc* during shake cultivation. Afterwards, the biomass of *Pc* without phenol addition was higher than the treatments that added Fe_3O_4 NPs or phenol (day 1 and day 2 of Fig. 2), which might be attributed to the toxicity

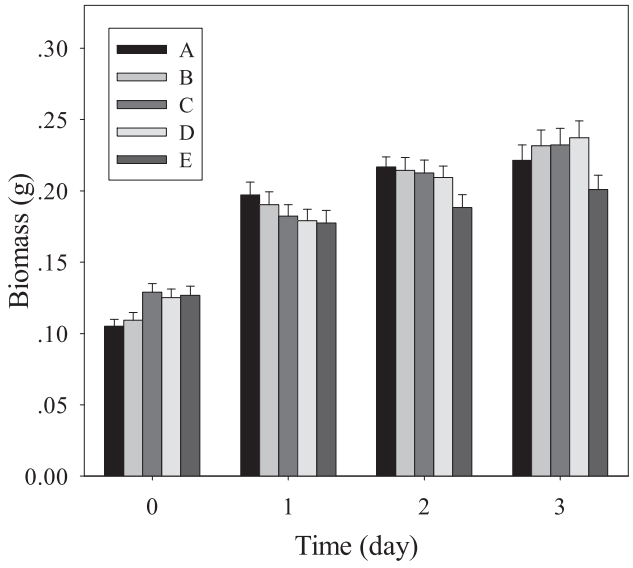

Fig. 2. Biomass changes in the treatments with different materials (A: *Pc*; B: *Pc* and 60 mg L^{-1} phenol; C: *Pc* and 0.5 g L^{-1} Fe_3O_4; D: *Pc*, 0.5 g L^{-1} Fe_3O_4 and 60 mg L^{-1} phenol; E: *Pc*, 0.5 g L^{-1} Fe_3O_4 and 120 mg L^{-1} phenol). The bars represent the standard deviations of the means ($n = 3$).

to *Pc* by Fe_3O_4 and phenol. However, the biomass in the treatments contained Fe_3O_4 NPs or 60 mg L^{-1} phenol increased on day 3, which was probably because of the removal of phenol and the adjustment of cell physiology with time increasing, whereas the treatments with 120 mg L^{-1} phenol maintained low biomass. This might because that excessive phenol addition still inhibited the activities of *Pc*.

Effect of Fe_3O_4 nanoparticles on phenol degradation

In order to investigate the effect of the amount of Fe_3O_4 NPs on the phenol degradation, the degradation efficiencies of phenol in the treatments with different amount of Fe_3O_4 NPs under both light and dark conditions were studied (Fig. 3). Phenol concentrations in all of the treatments were 60 mg L^{-1}. It was evident that the degradation efficiencies of phenol increased with the increase of time. It was further found that the phenol degradation under light was strongly dependent on Fe_3O_4 NPs concentration. In the low range, the phenol degradation efficiency was enhanced significantly with the increase of Fe_3O_4 NPs concentration, but was inhibited greatly with an excessive amount of NPs. Obviously, there should be an optimal amount of Fe_3O_4 NPs to achieve the best performance of phenol degradation. And the maximal peak value of phenol degradation efficiency (93.41%) on day 3 was detected at 0.5 g L^{-1} Fe_3O_4 NPs (Fig. 3a). However, the phenol degradation efficiency at 0.7 g L^{-1} NPs reached a peak on day 3 under dark, and the degradation efficiency was 40.36%. Furthermore, just a faint fluctuation in phenol degradation efficiency was observed on day 1 and day 2 (Fig. 3b). Fe_3O_4 NPs played an important role in the composite system. Fe_3O_4 NPs coexisted with oxalate could efficiently enhance the degradation of phenol under light condition via the formation of •OH with higher redox potential as described by the equations below (Lei et al., 2006; Xu et al., 2012a), thereby possibly affecting the degradation of phenol.

$$\text{Iron oxide} + nH_2C_2O_4 \leftrightarrow \left[\equiv Fe(C_2O_4)_n\right]^{(2n-3)-} \quad (1)$$

$$\left[\equiv Fe(C_2O_4)_n\right]^{(2n-3)-} + h\nu \rightarrow Fe(C_2O_4)_2^{2-}\left(\text{or}\equiv Fe(C_2O_4)_2^{2-}\right) + CO_2\cdot^- \quad (2)$$

$$Fe^{III}(C_2O_4)_n^{3-2n} + h\nu \rightarrow \left[Fe^{II}(C_2O_4)_{n-1}\right]^{4-2n} + C_2O_4\cdot^- \quad (3)$$

$$C_2O_4\cdot^- \rightarrow CO_2 + CO_2\cdot^- \quad (4)$$

$$CO_2\cdot^- + O_2 \rightarrow CO_2 + O_2\cdot^- \quad (5)$$

$$O_2\cdot^- + Fe^{3+} \rightarrow Fe^{2+} + O_2 \quad (6)$$

$$O_2\cdot^- + nH^+ + Fe^{2+} \rightarrow Fe^{3+} + H_2O_2 \quad (7)$$

$$Fe^{2+} + H_2O_2 \rightarrow Fe^{3+} + OH^- + \cdot OH \quad (8)$$

In this study, the degradation efficiencies of phenol under light were higher than that under the dark in three days (Fig. 3). This was because that phenol was mainly removed through biological adsorption and biological degradation under dark condition, while it was also effectively photodegraded by the photocatalyst formed by Fe_3O_4 NPs and oxalate as the equations described above under

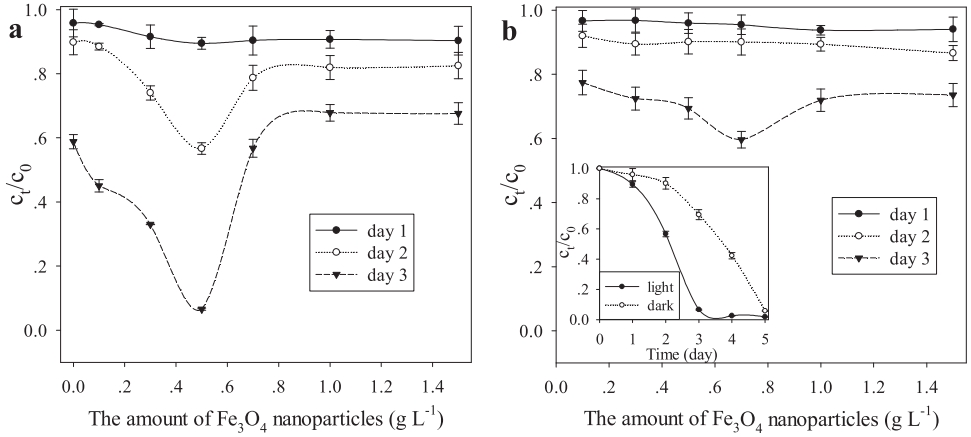

Fig. 3. Changes of phenol degradation at different concentrations of Fe_3O_4 NPs under light (a) and dark (b) condition. Phenol concentrations in all of the treatments were 60 mg L^{-1}. The bars represent the standard deviations of the means ($n = 3$).

light condition. Moreover, the inserted figure therein (Fig. 3b) displayed the dependence of phenol degradation on time under light and dark condition, respectively. The results showed that the degradation of phenol under light condition was quite faster than that under dark condition in three days. However, the degradation efficiency of phenol on day 5 under dark also achieved 94.24%, which was close to that under light (98.22%). This was probably because that irradiation had no pronounced effect on the catalytic decomposition capacity, but the rate of degradation was fast in the presence of light, which was proved by Khedr et al. (Khedr et al., 2009).

Effect of initial phenol concentration on phenol degradation

To investigate the effect of initial concentration of phenol on its degradation, a set of experiments were carried out with initial concentration of phenol varying from 0 to 120 mg L^{-1} in the presence of 0.5 g L^{-1} Fe_3O_4 NPs under light condition. Phenol degradation efficiencies under light condition in the treatments with different phenol concentrations and the treatments with different materials varied during shake cultivation (Fig. 4). It was apparent that the degradation efficiencies of phenol increased with the increase of time. And the phenol degradation efficiencies gradually elevated with an increase in phenol concentration, which confirmed that the increase of initial concentration of phenol had a promotion to its degradation. Besides, all of the degradation efficiencies were higher than 80% on day 3 (Fig. 4a). In addition, when phenol concentration was 60 mg L^{-1}, the degradation of phenol by Fe_3O_4 NPs-*Pc*-oxalate composite system was much higher than other three treatments which used Fe_3O_4 NPs, Fe_3O_4 NPs-oxalate, *Pc*, respectively (Fig. 4b). Obviously, the composite system could degrade phenol effectively.

Participation of oxalate in the composite system

Pc can secrete oxalate during its growth in both liquid and solid culture medium (Dutton et al., 1993; Galkin et al., 1998; Mäkelä et al., 2002). Oxalate secreted by *Pc* provides many advantages for their growth and colonization of substrates, and it plays an important role in white-rot decay system. Oxalate concentrations at different concentrations of Fe_3O_4 NPs (Fig. 5a) and at different phenol concentrations (Fig. 5b) under light condition varied during shake cultivation. Phenol concentrations were 60 mg L^{-1} in Fig. 5a and Fe_3O_4 NPs concentrations were 0.5 g L^{-1} in Fig. 5b. The biomass in the treatment with 0.5 g L^{-1} Fe_3O_4 NPs and 60 mg L^{-1} phenol was 0.1791 g on day 1, 0.2094 g on day 2, 0.2373 g on day 3, and the biomass in the treatment with 0.5 g L^{-1} Fe_3O_4 NPs and 120 mg L^{-1} phenol was 0.1775 g on day 1, 0.1883 g on day 2, 0.2009 g on day 3. Fig. 5 showed that oxalate concentration was high, this was probably because that phenol was added into the composite system after *Pc* was cultured for three days, and oxalate could accumulate in the composite system continuously, on the other hand, oxalate production would reach a peak after 4–5 days cultivation, that was to say, oxalate concentration was relatively high on about day 2 after phenol addition. From Fig. 5a, when the concentration of Fe_3O_4 NPs was in the low range, oxalate accumulations increased with an increase in NPs concentration and they reached a peak in 0.5 g L^{-1} NPs on all days. Obviously, *Pc* could maintain good activities under Fe_3O_4 NPs stress. This observation was in good agreement with previous findings reporting that Fe_3O_4 NPs showed low toxicity and favorable biocompatibility when coexisted with *Pc* (Xu et al., 2012a,b). Afterward, oxalate secretions decreased with the increase of NPs concentration, which was because that oxalate was absorbed by excessive Fe_3O_4 NPs and reacted as described by Eq. (1) in section "Effect of Fe_3O_4 nanoparticles on phenol degradation". Besides, the oxalate accumulations peaked together with phenol degradation efficiencies under light condition (Figs. 5a and 3a), which indicated that adequate oxalate could enhance the degradation of phenol. And it was ascribed to the participation of oxalate in the photocatalytic process. Fig. 5b displayed oxalate concentrations in the treatments with different phenol concentrations. From Fig. 5b, it showed that the oxalate accumulations raised rapidly with the increase of phenol concentration on all days, which was because that the presence of phenol could greatly promote the secretion of oxalate. Another possible reason was that oxalate could form as an intermediate in the catalytic oxidation of phenol (Duprez et al., 1996). Additionally, from Figs. 4a and 5b, it displayed that the degradation efficiency of phenol increased with oxalate production, which showed that the presence of oxalate could accelerate the degradation of phenol, and that was also in good agreement with the results discussed in Fig. 5a.

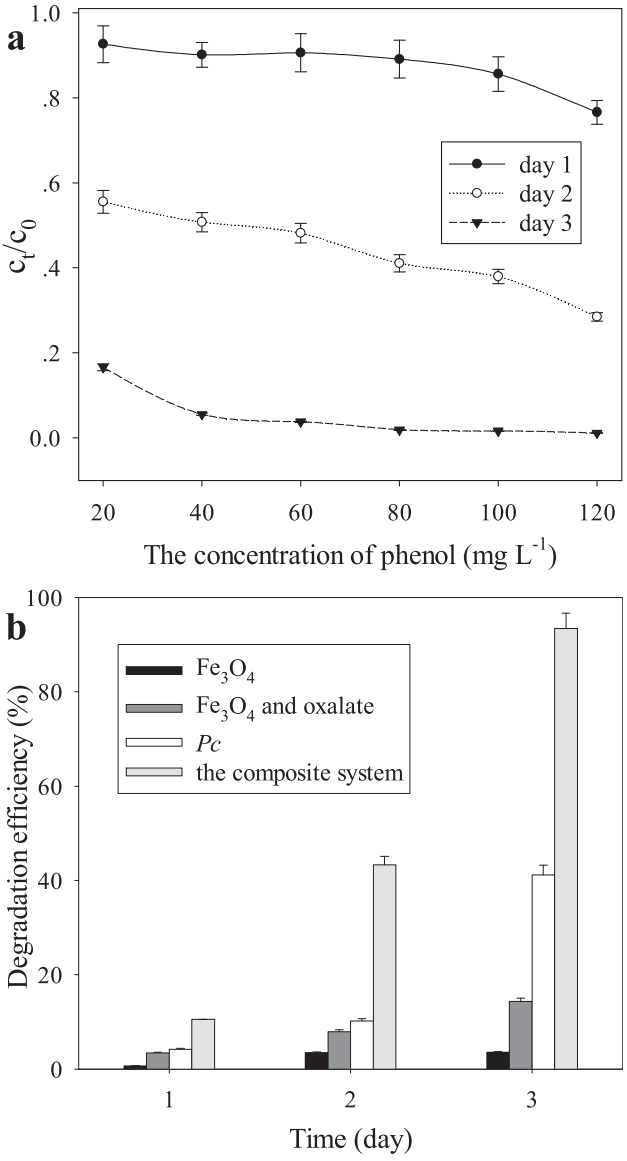

Fig. 4. Changes of phenol degradation under light condition in the treatments with different phenol concentrations (a) and the treatments with different materials (60 mg L^{-1} phenol) (b), respectively. The bars represent the standard deviations of the means ($n = 3$).

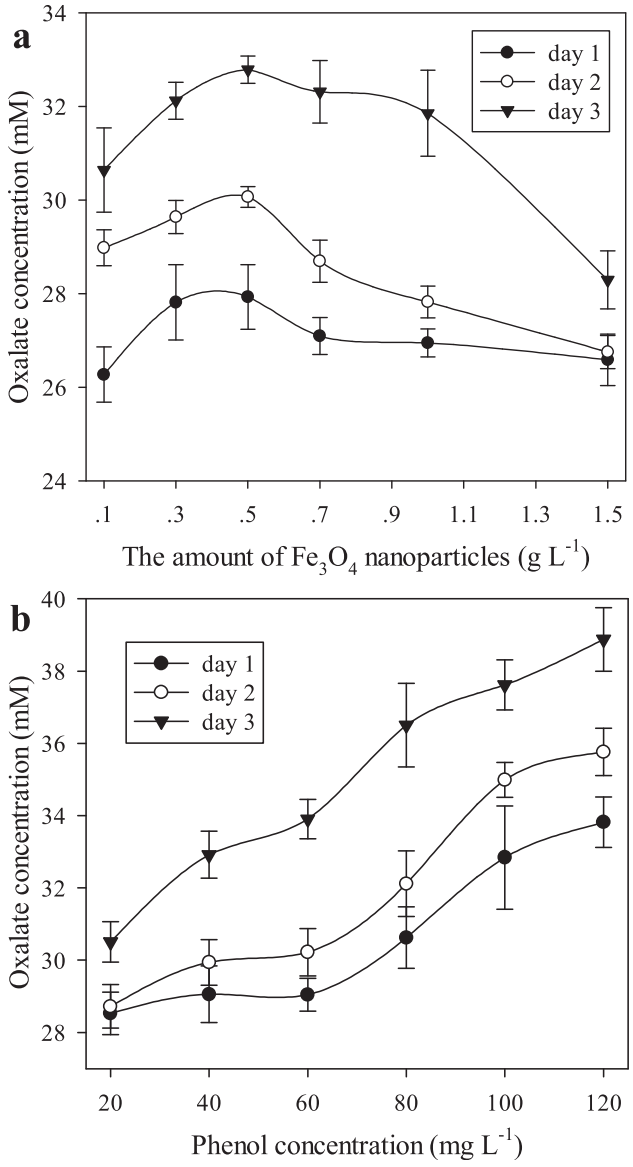

Fig. 5. Oxalate secretion of *Pc* under light condition detected in substrate filtrate at different concentrations of Fe_3O_4 NPs (a) and at different phenol concentrations (b). Phenol concentrations were 60 mg L^{-1} in Fig. 5a and Fe_3O_4 NPs concentrations were 0.5 g L^{-1} in Fig. 5b. The bars represent the standard deviations of the means ($n = 3$).

Enzymatic-based degradation process in the composite system

LiP and MnP, secreted by *Pc*, could catalyze the degradation of a wide variety of organic pollutants (Bumpus et al., 1985; Barr and Aust, 1994). MnP is considered to be the most common lignin-modifying peroxidase produced by almost all wood-colonizing basidiomycetes and involved in the initial attack of lignin by Mn^{3+} chelate complexes (Hofrichter, 2002; Martínez et al., 2005). LiP is the first discovered enzyme that catalyzes the partial depolymerization of methylated lignin in vitro (Tien and Kirk, 1983). Lac has been confirmed to be essential for ligninolytic activity in many white-rot fungi (Leonowicz et al., 2001). However, Lac alone are unable to oxidize some substances due to their lower redox potential relative to fungal peroxidases (Kurniawati and Nicell, 2007; Huang et al., 2008; Liu et al., 2012). In addition, the activities of Lac are very low. Furthermore, the extracellular non-specific and non-stereoselective ligninolytic system of *Pc* is composed of LiP and MnP, which function together with H_2O_2 producing oxidases and secondary metabolites (Singh and Pakshirajan, 2010), therefore LiP and MnP activities were studied. LiP and MnP activities in the treatments with different initial phenol concentrations in the presence of 0.5 g L^{-1} Fe_3O_4 NPs were presented in Fig. 6. High levels of MnP activities and low levels of LiP activities were observed. Time and phenol concentration-dependent MnP activities have been found during the whole degradation process. The activities of MnP raised rapidly with the increase of phenol concentration on day 2 and day 3 (Fig. 6b). These results indicated that *Pc* could maintain good activities of MnP under phenol stress, which was attributed to the resistant character to pollutants of *Pc*, and similar result about the resistant character of *Pc* was also reported (Huang et al., 2010b). Besides, high levels of MnP activities were detected together with high degradation efficiencies (Figs. 6b and 4a), which displayed that high MnP activities contributed significantly to phenol degradation. However, the LiP activities increased at low initial phenol concentrations and it reached a peak (1.16 U L^{-1} on day 1, 1.69 U L^{-1} on day 2, 2.58 U L^{-1} on day 3) at 60 mg L^{-1} phenol concentration on all days, and then decreased when the initial

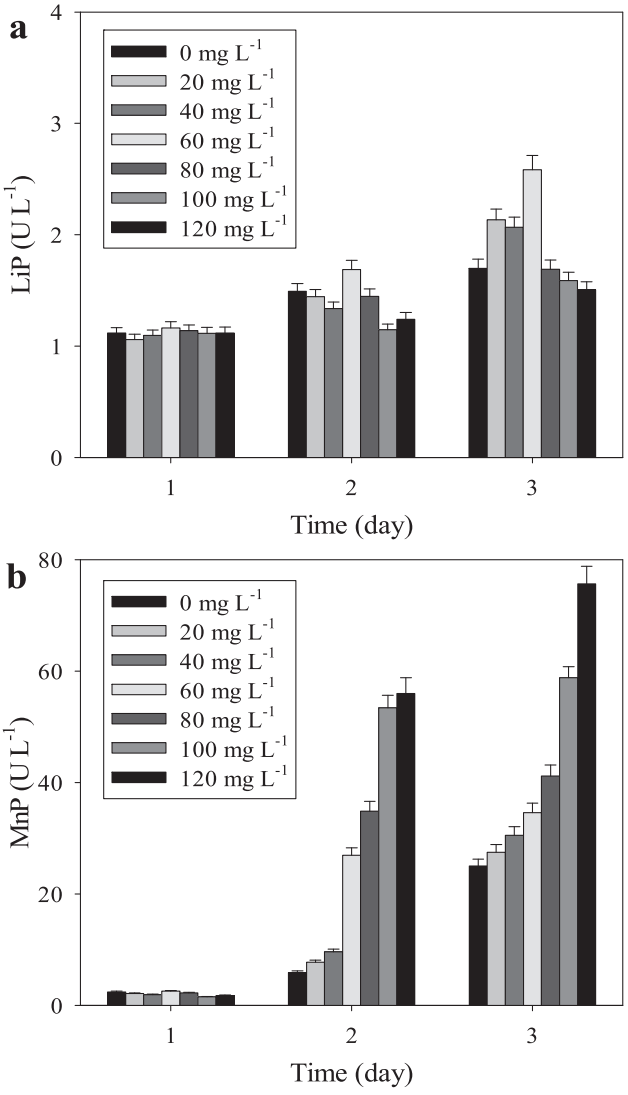

Fig. 6. Different phenol concentrations and time-dependent LiP (a) and MnP (b) activities by *Pc*. Fe_3O_4 NPs concentrations were 0.5 g L^{-1}. The bars represent the standard deviations of the means ($n = 3$).

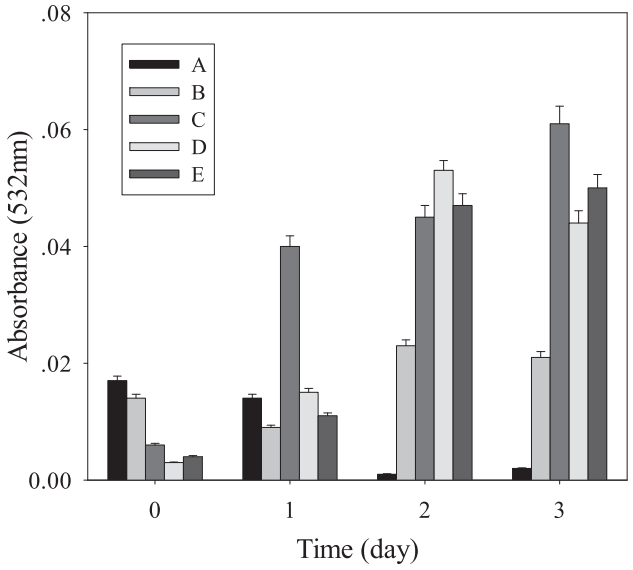

Fig. 7. Hydroxyl radicals changes in the treatments with different materials (A: *Pc*; B: *Pc* and 60 mg L^{-1} phenol; C: *Pc* and 0.5 g L^{-1} Fe_3O_4; D: *Pc*, 0.5 g L^{-1} Fe_3O_4 and 60 mg L^{-1} phenol; E: *Pc*, 0.5 g L^{-1} Fe_3O_4 and 120 mg L^{-1} phenol). The bars represent the standard deviations of the means ($n = 3$).

phenol concentrations were higher than 60 mg L^{-1}. But the LiP activities didn't display significant changes with the increase of phenol concentration on the whole (Fig. 6a), which indicated that the contribution of LiP to phenol degradation was smaller than that of MnP.

Moreover, from Fig. 6, it was displayed that MnP displayed a higher activities than that of LiP, and similar results were also shown by Arora et al. (Arora et al., 2002) and Li et al. (Li et al., 2011). MnP activities increased together with oxalate concentrations (Figs. 6b and 5b), which was probably due to the chelation and stabilization of Mn^{3+} by oxalic acid (Perez and Jeffries, 1993; Hofrichter et al., 1999; Li et al., 2011). And low LiP activities might be due to the inhibition to LiP in the extracellular site by oxalate (Akamatsu et al., 1990; Li et al., 2011).

Production of hydroxyl radicals

The •OH was produced during shake cultivation as described above (Eq. (1) to Eq. (8) in section "Effect of Fe_3O_4 nanoparticles on phenol degradation"), and it could be produced by ligninolytic enzymes (Halliwell, 1965). Hydroxyl radicals production in the various samples (*Pc*; *Pc* and 60 mg L^{-1} phenol; *Pc* and 0.5 g L^{-1} Fe_3O_4; *Pc*, 0.5 g L^{-1} Fe_3O_4 and 60 mg L^{-1} phenol; *Pc*, 0.5 g L^{-1} Fe_3O_4 and 120 mg L^{-1} phenol) varied during degradation process (Fig. 7). The results showed that •OH production in the samples contained

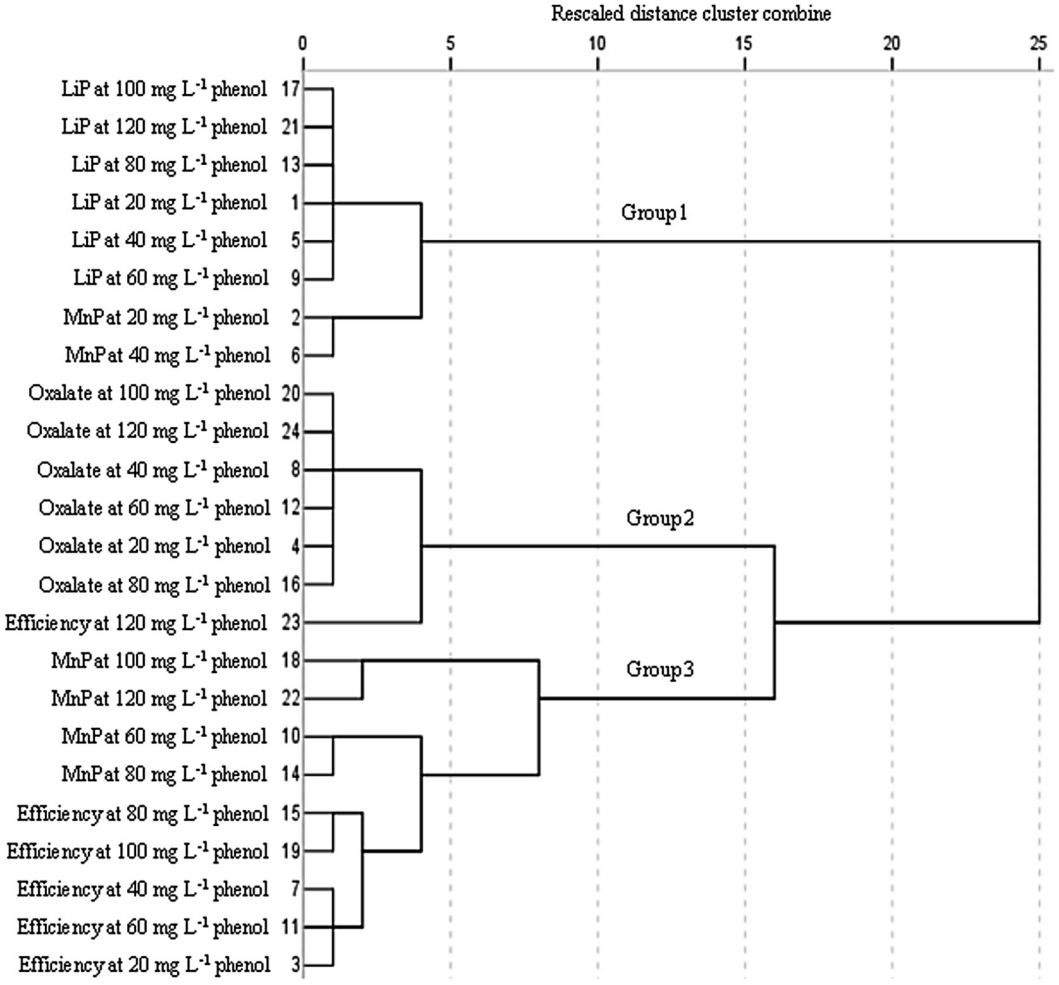

Fig. 8. Classification of some indexes (degradation efficiency, oxalate concentration, LiP activity and MnP activity) at different phenol concentrations by cluster analysis based on the similarity measures between the values of different indexes in different groups. Between-groups linkage was used as cluster method.

Fe_3O_4 NPs increased rapidly with the increase of time (C, D, E in Fig. 7). However, after phenol addition, •OH production in the sample contained *Pc* and phenol (sample B) just displayed a faint fluctuation, and the production of •OH was much less than the samples that added Fe_3O_4 NPs. This confirmed that the treatments added Fe_3O_4 could promote the genetation of •OH as Fe_3O_4 NPs coexisted with oxalate could generate •OH after a sequence of reactions under light condition (Eq. (1) to Eq. (8) in section "Effect of Fe_3O_4 nanoparticles on phenol degradation"). In addition, when phenol added, •OH decreased via reacted with phenol (Fig. 7).

Statistical analysis and degradation mechanism analysis

Cluster analysis was conducted to classify four indexes related to degradation efficiency at different phenol concentrations (Fig. 8). Three groups were obtained. Efficiency at 120 mg L^{-1} phenol and oxalate at 120 mg L^{-1} phenol belonged to the same group, which indicated that the effect of phenol on these indexes were similar, suggesting that oxalate was the main factor that influenced the degradation of phenol when the phenol concentration was 120 mg L^{-1}. Similarly, we could know that MnP affected phenol degradation to a large extent when phenol concentration ranged from 60 to 100 mg L^{-1}.

In this study, iron oxide could absorb oxalate and react as described by equations in section Effect of Fe_3O_4 nanoparticles on phenol degradation, it was obvious that Fe^{2+} was oxidized to Fe^{3+} in the composite system. Besides, we found that the color of NPs changed into reddish brown after coexisted with phenol for 3 days in the experiments, which was in good agreement with the theory that Fe^{2+} was oxidized to Fe^{3+}. NPs was continuously consumed due to the irreversible reaction, therefore the system did not continue to be used repeatedly after phenol degradation. However, the experiments in different concentrations of Fe_3O_4 NPs and different concentrations of phenol were conducted repeatedly for many times and *Pc* could maintain good activities under phenol stress.

The possible degradation mechanism in the composite system was showed on Fig. 9. Phenol was mainly degraded by biodegradation and photocatalysis in the composite system under light condition. Oxalate secreted by *Pc* coexisted with Fe_3O_4 NPs under light condition could efficiently enhance phenol degradation through the formation of •OH as described by the equations in Effect of Fe_3O_4 nanoparticles on phenol degradation, thus phenol could be degraded effectively. Meanwhile, LiP and MnP could also catalyze the degradation of phenol. The results of cluster analysis displayed that oxalate and ligninolytic enzymes activities were the main factors that effected phenol degradation, and Fe_3O_4 NPs also strongly influenced the degradation efficiency of phenol (Fig. 3a), which demonstrated that both the biodegradation and photocatalysis played part in the degradation process, that is to say, the degradation of phenol in the composite system was accomplished under the coupling of abiotic and biotic degradation. However, further studies are needed to investigate the detail degradation mechanism in the composite system because the mechanism was not very certain in this study.

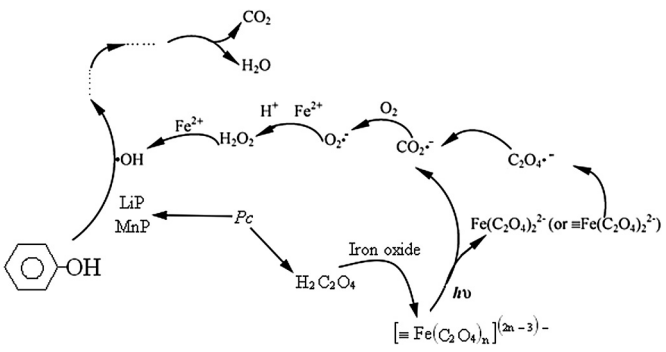

Fig. 9. The mechanism of the phenol degradation.

Conclusions

A novel composite system, which combined biological degradation with photocatalytic degradation, was set up at the presence of Fe_3O_4 NPs and white rot fungus (*Pc*) together with its secretion oxalate in the present study. And phenol could be effectively degraded via the coupled photocatalytic-biological process in this composite system under solar light. The degradation efficiency of phenol under light was higher than that under dark condition. Besides, phenol degradation efficiency reached a peak after 3 days' shake cultivation when the amount of Fe_3O_4 NPs was 0.5 g L^{-1} under light condition, whereas the maximal peak value of phenol degradation efficiency on day 3 under dark was detected at 0.7 g L^{-1} Fe_3O_4 NPs. Additionally, oxalate was found to be strongly dependent on Fe_3O_4 NPs concentration and adequate oxalate could accelerate phenol degradation due to the participation of oxalate in the photocatalytic process. Furthermore, the increase of initial phenol concentration had a promotion to its degradation when phenol concentration ranged from 20 to 120 mg L^{-1} under light. In addition, high levels of MnP activities and low levels of LiP activities were obtained at different phenol concentrations under light condition, and the contribution of MnP to phenol degradation was greater than that of LiP. Importantly, the obtained results were available to demonstrate that coupling of both biodegradation and photocatalysis played part in the phenol degradation process. The present findings proposed a new method of treatment of phenol wastewater and could provide useful references for promoting more efficient treatment of phenol wastewater.

Acknowledgments

The study was financially supported by the Program for the National Natural Science Foundation of China (51039001, 51278176, 51408206), the Research Fund for the Doctoral Program of Higher Education of China (20100161110012), the Program for New Century Excellent Talents in University (NCET-13-0186), the Fundamental Research Funds for the Central Universities and Hunan University Fund for Multidisciplinary Developing (531107040762).

References

Afkhami, A., Saber-Tehrani, M., Bagheri, H., 2010. Modified maghemite nanoparticles as an efficient adsorbent for removing some cationic dyes from aqueous solution. Desalination 263, 240–248.
Akamatsu, Y., Ma, D.B., Higuchi, T., Shimada, M., 1990. A novel enzymatic decarboxylation of oxalic acid by the lignin peroxidase system of white-rot fungus *Phanerochaete chrysosporium*. FEBS Lett. 269, 261–263.
Arora, D.S., Chander, M., Gill, P.K., 2002. Involvement of lignin peroxidase, manganese peroxidase and laccase in degradation and selective ligninolysis of wheat straw. Int. Biodeterior. Biodegrad. 50, 115–120.
Barr, D.P., Aust, S.D., 1994. Mechanisms white rot fungi use to degrade pollutants. Environ. Sci. Technol. 28, 78–87.
Bumpus, J.A., Tien, M., Wright, D., Aust, S.D., 1985. Oxidation of persistent environmental pollutants by a white rot fungus. Science 228, 1434–1436.
Chung, T.P., Tseng, H.Y., Juang, R.S., 2003. Mass transfer effect and intermediate detection for phenol degradation in immobilized *Pseudomonas putida* systems. Process Biochem. (Amst. Neth) 38, 1497–1507.
Duprez, D., Delanoë, F., Barbier Jr., J., Isnard, P., Blanchard, G., 1996. Catalytic oxidation of organic compounds in aqueous media. Catal. Today 29, 317–322.
Dutton, M.V., Evans, C.S., Atkey, P.T., Wood, D.A., 1993. Oxalate production by basidiomycetes, including the white-rot species *Coriolus versicolor* and *Phanerochaete chrysosporium*. Appl. Microbiol. Biotechnol. 39, 5–10.

Faust, B.C., Zepp, R.G., 1993. Photochemistry of aqueous iron (III)-polycarboxylate complexes: roles in the chemistry of atmospheric and surface waters. Environ. Sci. Technol. 27, 2517–2522.
Galkin, S., Vares, T., Kalsi, M., Hatakka, A., 1998. Production of organic acids by different white-rot fungi as detected using capillary zone electrophoresis. Biotechnol. Tech. 12, 267–271.
Halliwell, B., Gutteridge, J.M.C., Grootveld, M., 1985. Handbook of Methods for Oxygen Radical Research. CRC Press, Boca Raton, pp. 177–180.
Halliwell, G., 1965. Catalytic decomposition of cellulose under biological conditions. Biochem. J. 95, 35–40.
Hofrichter, M., Vares, T., Kalsi, M., Galkin, S., Scheibner, K., Fritsche, W., Hatakka, A., 1999. Production of manganese peroxidase and organic acids and mineralization of ^{14}C-labelled lignin (^{14}C-DHP) during solid-state fermentation of wheat straw with the white rot fungus *Nematoloma frowardii*. Appl. Environ. Microbiol. 65, 1864–1870.
Hofrichter, M., 2002. Review: lignin conversion by manganese peroxidase (MnP). Enzyme Microb. Technol. 30, 454–466.
Huang, D.L., Zeng, G.M., Feng, C.L., Hu, S., Jiang, X.Y., Tang, L., Su, F.F., Zhang, Y., Zeng, W., Liu, H.L., 2008. Degradation of lead-contaminated lignocellulosic waste by *Phanerochaete chrysosporium* and the reduction of lead toxicity. Environ. Sci. Technol. 42, 4946–4951.
Huang, D.L., Zeng, G.M., Feng, C.L., Hu, S., Lai, C., Zhao, M.H., Su, F.F., Tang, L., Liu, H.L., 2010a. Changes of microbial population structure related to lignin degradation during lignocellulosic waste composting. Bioresour. Technol. 101, 4062–4067.
Huang, D.L., Zeng, G.M., Feng, C.L., Hu, S., Zhao, M.H., Lai, C., Zhang, Y., Jiang, X.Y., Liu, H.L., 2010b. Mycelial growth and solid-state fermentation of lignocellulosic waste by white-rot fungus *Phanerochaete chrysosporium* under lead stress. Chemosphere 81, 1091–1097.
Huang, D.L., Zeng, G.M., Jiang, X.Y., Feng, C.L., Yu, H.Y., Huang, G.H., Liu, H.L., 2006. Bioremediation of Pb-contaminated soil by incubating with *Phanerochaete chrysosporium* and straw. J. Hazard. Mater. B 134, 268–276.
Khedr, M.H., Abdel Halim, K.S., Soliman, N.K., 2009. Synthesis and photocatalytic activity of nano-sized iron oxides. Mater. Lett. 63, 598–601.
Kibret, M., Somitsch, W., Robra, K.H., 2000. Characterization of a phenol degrading mixed population by enzyme assay. Water Res. 34, 1127–1134.
Kirk, T.K., Schultz, E., Connors, W.J., Lorenz, L.F., Zeikus, J.G., 1978. Influence of culture parameters on lignin metabolism by *Phanerochaete chrysosporium*. Archiv. Microbiol. 117, 277–285.
Kurniawati, S., Nicell, J.A., 2007. Efficacy of mediators for enhancing the laccase-catalyzed oxidation of aqueous phenol. Enzyme Microb. Technol. 41, 353–361.
Lai, C., Zeng, G.M., Huang, D.L., Zhao, M.H., Huang, H.L., Huang, C., Wei, Z., Li, N.J., Xu, P., Zhang, C., Xie, G.X., 2013. Effect of ABTS on the adsorption of Trametes versicolor laccase on alkali lignin. Int. Biodeterior. Biodegrad. 82, 180–186.
Lei, J., Liu, C.S., Li, F.B., Li, X.M., Zhou, S.G., Liu, T.X., Gu, M.H., Wu, Q.T., 2006. Photodegradation of orange I in the heterogeneous iron oxide–oxalate complex system under UVA irradiation. J. Hazard. Mater. B 137, 1016–1024.
Leland, J.K., Bard, A.J., 1987. Photochemistry of colloidal semiconducting iron oxide polymorphs. J. Chem. Phys. 91, 5076–5083.
Leonowicz, A., Cho, N.-S., Luterek, J., Wilkolazka, A., Wojtas-Wailewska, M., Matuszewska, A., Hofrichter, M., Wesenberg, D., Rogalski, J., 2001. Fungal laccase: properties and activity on lignin. J. Basic Microbiol. 41, 185–227.
Li, N.J., Zeng, G.M., Huang, D.L., Hu, S., Feng, C.L., Zhao, M.H., Lai, C., Huang, C., Wei, Z., Xie, G.X., 2011. Oxalate production at different initial Pb^{2+} concentrations and the influence of oxalate during solid-state fermentation of straw with *Phanerochaete chrysosporium*. Bioresour. Technol. 102, 8137–8142.
Liu, Y.Y., Zeng, Z.T., Zeng, G.M., Tang, L., Pang, Y., Li, Z., Liu, C., Lei, X.X., Wu, M.S., Ren, P.Y., Liu, Z.F., Chen, M., Xie, G.X., 2012. Immobilization of laccase on magnetic bimodal mesoporous carbon and the application in the removal of phenolic compounds. Bioresour. Technol. 115, 21–26.
Mäkelä, M., Galkin, S., Hatakka, A., Lundell, T., 2002. Production of organic acids and oxalate decarboxylase in lignin-degrading white rot fungi. Enzyme Microb. Technol. 30, 542–549.
Martínez, A.T., Speranza, M., Ruiz-Duenas, F.J., Ferreira, P., Guillén, F., Martínez, M.J., Gutiérrez, A., del Rio, C.J., 2005. Biodegradation of lignocellulosics: microbial, chemical, and enzymatic aspects of the fungal attack of lignin. Int. Microbiol. 8, 195–204.
Martínková, L., Uhnáková, B., Pátek, M., Nešvera, J., Křen, V., 2009. Biodegradation potential of the genus Rhodococcus. Environ. Int. 35, 162–177.
McHenry, M.E., Laughlin, D.E., 2000. Nano-scale materials development for future magnetic applications. Acta Mater. 48, 223–238.
Nair, C.I., Jayachandran, K., Shashidhar, S., 2008. Biodegradation of phenol. Afr. J. Biotechnol. 7, 4951–4958.
Pan, B.J., Qiu, H., Pan, B.C., Nie, G.Z., Xiao, L.L., Lv, L., Zhang, W.M., Zhang, Q.X., Zheng, S.R., 2010. Highly efficient removal of heavy metals by polymer-supported nanosized hydrated Fe (III) oxides: behavior and XPS study. Water Res. 44, 815–824.
Perez, J., Jeffries, T.W., 1993. Role of organic acid chelators in manganese regulation of lignin degradation by *Phanerochaete chrysosporium*. Appl. Biochem. Biotechnol. 39, 227–238.
Shaari, N., Tan, S.H., Mohamed, A.R., 2012. Synthesis and characterization of CNT/Ce-TiO_2 nanocomposite for phenol degradation. J. Rare Earths 30, 651–658.
Siffert, C., Sulzberger, B., 1991. Light-induced dissolution of hematite in the presence of oxalate. A case study. Langmuir 7, 1627–1634.
Singh, S., Pakshirajan, K., 2010. Enzyme activities and de colourization of single and mixed azo dyes by the white-rot fungus *Phanerochaete chrysosporium*. Int. Biodeterior. Biodegrad. 64, 146–150.
Tien, M., Kirk, T.K., 1983. Lignin-degrading enzyme from the hymenomycete *Phanerochaete chrysosporium* burds. Science 221, 661–663.
Tien, M., 1988. Lignin peroxidase of *Phanerochaete chrysosporium*. Methods Enzym. 161, 238–249.
Wariishi, H., Valli, K., Gold, M.H., 1992. Manganese (II) oxidation by manganese peroxidase from the basidiomycete *Phanerochaete chrysosporium*. Kinetic mechanism and role of chelators. J. Biolo. Chem. 267, 23688–23695.
Xu, P., Zeng, G.M., Huang, D.L., Hu, S., Feng, C.L., Lai, C., Zhao, M.H., Huang, C., Li, N.J., Wei, Z., Xie, G.X., 2013. Synthesis of iron oxide nanoparticles and their application in *Phanerochaete chrysosporium* immobilization for Pb (II) removal. Colloids Surf. A: Physicochem. Eng. Asp. 419, 147–155.
Xu, P., Zeng, G.M., Huang, D.L., Feng, C.L., Hu, S., Zhao, M.H., Lai, C., Wei, Z., Huang, C., Xie, G.X., Liu, Z.F., 2012a. Use of iron oxide nanomaterials in wastewater treatment: a review. Sci. Total Environ. 424, 1–10.
Xu, P., Zeng, G.M., Huang, D.L., Lai, C., Zhao, M.H., Wei, Z., Li, N.J., Huang, C., Xie, G.X., 2012b. Adsorption of Pb (II) by iron oxide nanoparticles immobilized *Phanerochaete chrysosporium*: equilibrium, kinetic, thermodynamic and mechanisms analysis. Chem. Eng. J. 203, 423–431.
Zhao, M.H., Zeng, Z.T., Zeng, G.M., Huang, D.L., Feng, C.L., Lai, C., Huang, C., Wei, Z., Li, N.J., Xu, P., Zhang, C., Liu, Z.F., Xie, G.X., 2012. Effects of ratio of manganese peroxidase to lignin peroxidase on transfer of ligninolytic enzymes in different composting substrates. Biochem. Eng. J. 67, 132–139.